Accepted Manuscript

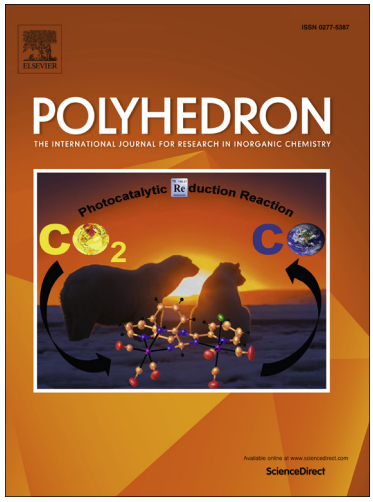

Spectroscopic and TD- DFT Studies on the Turn-off Fluorescent Chemosensor based on Anthraldehyde N(4) Cyclohexyl Thiosemicarbazone for the Selective Recognition of Fluoride and Copper Ions

Sabeel M. Basheer, Anthony C. Willis, Ron J. Pace, Anandaram Sreekanth

PII: S0277-5387(16)00035-8
DOI: http://dx.doi.org/10.1016/j.poly.2016.01.021
Reference: POLY 11783

To appear in: *Polyhedron*

Received Date: 21 October 2015
Accepted Date: 20 January 2016

Please cite this article as: S.M. Basheer, A.C. Willis, R.J. Pace, A. Sreekanth, Spectroscopic and TD- DFT Studies on the Turn-off Fluorescent Chemosensor based on Anthraldehyde N(4) Cyclohexyl Thiosemicarbazone for the Selective Recognition of Fluoride and Copper Ions, *Polyhedron* (2016), doi: http://dx.doi.org/10.1016/j.poly.2016.01.021

Spectroscopic and TD- DFT Studies on the Turn-off Fluorescent Chemosensor based on Anthraldehyde N(4) Cyclohexyl Thiosemicarbazone for the Selective Recognition of Fluoride and Copper Ions

Sabeel M. Basheer[a], Anthony C. Willis[b], Ron J. Pace[b], Anandaram Sreekanth *[a]

Abstract: The copper and fluoride ions sensing mechanism of a chemosensor based on anthraldehyde N(4) cyclohexyl thiosemicarbazone (AntCy) was investigated via colorimetric, fluorescence, electrochemical and NMR titration studies. Detailed investigations on their sensing mechanism was done using DFT and TD-DFT studies. ^{1}H NMR titration shows deprotonation of NH protons by fluoride ion is a prominent step in naked eye recognition. The Gibbs free energy of overall sensing reaction has moderate transition barrier with 18.19 Kcal mol^{-1}. Using the vibrational frequency analysis, all the local minima of ground state and excited state were confirmed. Due to the small size and strong electronegativity of fluoride, an intramolecular hydrogen bonding interaction with N(3)-H, which is closer to anthracene moiety was found to be preferentially formed. The excited state proton transfer mechanism was further confirmed with donor–acceptor interactions using Natural Bond Orbital (NBO) analysis and Potential Energy Surface (PES) analysis. The ICT mechanism for copper ion sensing was also confirmed with TD-DFT calculations.

Key Words: Fluoride sensor, Thiosemicarbazone, PET, TD-DFT, Fluorescence, ^{1}H-NMR

[a] Department of Chemistry, National Institute of Technology, Tiruchirappalli - 620 015, India.

*Corresponding Author: E-mail address: sreekanth@nitt.edu; Tel: +91 431 2503642

[b]Research School of Chemistry, The Australian National University, Canberra, ACT 2601, Australia

CCDC: 1431947 contains the supplementary crystallographic data for AntCy. These data can be obtained free of charge via http://www.ccdc.cam.ac.uk/conts/retrieving.html, or from the Cambridge Crystallographic Data Centre, 12 Union Road, Cambridge CB2 1EZ, UK; fax: (+44) 1223-336-033; or e mail: deposit@ccdc.cam.ac.uk.

1. Introduction

Chemosensors with high selectivity and sensitivity through optical response appear to be particularly attractive due to their simplicity in recognition methods and accuracy [1-4]. Detection and recognition of fluoride is of unique interest owing to its roles in a broad range of biological, chemical and medicinal processes such as preventing dental caries and osteoporosis, fluorination of drinking water and chemical and nuclear warfare agents [5,6]. The fluoride toxicity is exposed on a less salubrious level to result in fluorosis in terms of increasing bone density. Among the cations, the copper ion is important in enzyme catalysed reactions because of its distinct effects in neurologic system and results pathological disease prevention protein misfolding and in several neurodegenerative diseases [59-62]. The sensing of F^- and Cu^{2+} ion give apparent advantages such as operational simplicity, high selectivity-sensitivity and rapid implementation [7-15].

Fluoride with its high electron density and large electronegativity, prefers to form stronger hydrogen bonds with receptors [16,17]. N-H---F^- interactions are well reported [18,19]. Chemosensors based on thio-urea derivatives have gained more attention due to the presence of strong hydrogen donors to evoke potential hydrogen bond formation. According to Irving-Williams stability series, the presence of sulphur atom increases the affinity for soft metal ion such as Cu^{2+}. The sensing mechanisms are mainly classified into either electron transfer (ET) or charge transfer (CT) or energy transfer (ET) or excimer/exciplex interaction [20-23]. The intramolecular charge transfer (ICT), metal to ligand charge transfer (MLCT) and twisted intramolecular charge transfer (TICT) are included in the charge transfer (CT) mechanism, while Photo-Induced electron transfer (PET) is the most widely seen electron transfer mechanism [24,25]. Fluorescence resonance energy transfer (FRET) and excited state proton transfer (ESPT) are the other two important mechanisms [26,27]. According to PET, chemosensor's electron pair is coordinated to external ions, then the electron transfer will be prevented and the fluorescence is switch on. Most of the benzenoid compounds [28] show this type of mechanism. When a receptor as an electron donor, is bound with the anion it alters the electron density distribution in the receptor, hence blue shift occurs. If the chemosensor is an electron receptor then the same electron density push-pull effect will result into red shift [24,25]. However, the theoretical studies on the mechanism for sensing anions are rare, especially for PET mechanism [29,33].

Previously, we have reported the experimental studies on selective anion sensing using the thiocarbohydrazone and thiosemicarbazones based Chemosensors [34-37]. Present work deal with the experimental studies and theoretical mechanism of chemosensing behaviour of thiosemicarbazone derivative towards selective fluoride and copper ion.

2. Experimental section

2.1 Preparation of AntCy

Ethanolic solutions of cyclohexyl isothiocyanate (0.706 g, 5 mmol) and hydrazine hydrate (0.250 g, 5 mmol) were mixed with constant stirring. The stirring was continued for 1 hr and then the white product, N(4)-cyclohexyl thiosemicarbazide formed was filtered, washed and dried (Yield: 91%, 0.788 g). This product (0.346 g, 2 mmol) was dissolved in methanol (30 mL) and was added to the 9-anthraldehyde (0.43 g, 2 mmol) dissolved in methanol (5 mL), and the reaction mixture was continuously reflux for 4 hrs after adding a drop of acetic acid. The reaction mixture was kept aside for slow evaporation at room temperature. After one week time, the product which has been formed was isolated. Further

the product isolated was recrystallized from acetonitrile and methanol. Yield: 84%, melting point: 196-198˚C. The scheme is as shown in S1. Colour: Pale Yellow, Yield: 81%, M.P 196-198^0 C, IR Data (cm^{-1}): 1530 (C=N), 1216 (C=S), ^{1}H NMR (400 MHz, DMSO-d6, ppm): 11.55 (1H, s, N-NH), 9.30 (1H, s, N-NH), 8.89 (1H, d, N=CH), 8.31 (9H, m, Ar-H), 2.57 (1H, m, N-CH) ^{13}C NMR (101 MHz, DMSO-d6, ppm): 32.31 (2C, m, C-C), ESI Mass: 362.2 (100%, m+1), 384.2 (Na+m, 50%), HRMS: 384.1508(Calculated), 384.1510 (Experimental) (Na+m, 100%). The detailed spectra were given in supporting data (S2-S6).

Fig 1 Structure of AntCy

2.2 Computational methods:

All calculations were performed using Gaussian 09 program [38]. The hybrid density functional theory (DFT) [39,40] and Time Dependent DFT (TD-DFT) calculations [41-44] were run for excited state as well as electronic spectra. The geometry optimisation of the chemosensor for the ground state (S_0) was obtained at the B3LYP using 6-31G+(d,p) basis set. The geometry optimisation of receptor-fluoride complex was also carried out with same method. Handy and co-workers' long range corrected version of B3LYP was used as Coulomb-attenuating method (CAM) hybrid function with long-range corrections (CAM-B3LYP) has been used to calculate the excitation energy (S_1) for more accuracy [45-49]. 6-31G+(d,p) basis set is moderate and suitable for such large organic compounds which is a proper basis set for ionic compound [50-52]. The transition states of hydrogen transfer located using Transition State (TS) calculations, with B3LYP/6-31G(d) basis set [53,54]. The receptor-copper complex was optimized with B3LYP/LanL2DZ method. In order to verify the nature of the transition state, intrinsic reaction coordinate calculations were carried out. The local minima of the ground state, Transition state, intermediate and excited state were confirmed with the vibrational frequency analysis. All electronic structure calculations were completed with no constrains for symmetry. To investigate the solvent effect of DMSO (Dielectric constant=46.826), PCM (Polarized Continuum Model) calculation was performed throughout the steps. The charge distribution, occupancy and energy of bonding orbitals were calculated using Natural Bond Orbital (NBO) approach at the same theoretical level as for the ground state and excited state geometry optimised structures [55]. The second order Fock matrix calculation was carried out to evaluate the donor–acceptor interactions in the NBO analysis. The mechanism was further confirmed with Potential energy Surface (PES) calculations.

2.3 X-ray crystallography

The crystal structure data collection of AntCy was done on a CrysAlias Pro., Agilent Technologies, Version 1.171.37.33d and the program used to solve the structure was SIR92, and the CRYSTALs was the program software used to refine the crystal structure at Australian National University, Canberra. The receptor A, $C_{22}H_{23}N_3S$ crystallizes in monoclinic $P2_{1/n}$ form with two independent molecules. Crystals of the compound were examined under a microscope and one was chosen which appeared to be single, of good quality and was of suitable size. It was mounted on X-ray diffractometer and its diffraction pattern was examined and found to be suitable for a single-crystal diffraction structure determination. A full intensity data set was collected on it. All data was collected with the graphite-monochromatic radiation of Mo Kα (λ=0.71073 Å). All hydrogen atoms were geometrically fixed and allowed to refine using a riding model. Absorption corrections were employed using multi ω scan with empirical absorption correction using spherical harmonics,

implemented in SCALE3 ABSPACK scaling algorithm. The crystallographic data along with details of structure solution refinements are given in Table 1.

Table 1. Crystal data and structure refinement parameters

3. Results & Discussions

The structural formula of AntCy is shown in Figure 1. It was well-characterized by elemental analyses, FT-IR, ^{1}H and ^{13}C NMR spectra and single crystal XRD studies. IR spectrum of the compound show the characteristic stretching frequencies at 1530 cm^{-1} attributed to ν(C=N) indicative of the newly formed azomethine group and bands at 1216 cm^{-1} assigned to ν(C=S) indicating that the thione form is dominating in the solid state. ^{1}H NMR of the AntCy shows singlet at 11.55 and 9.30 ppm for two different N-H protons which are found to disappear upon D_2O exchange.

3.1 Single crystal data of AntCy

The molecular structure of AntCy is shown in Fig. 2, and the important bond parameters were listed in Table 2. There are two crystallographically independent molecules in the asymmetric unit with bond lengths and angles agree to each other are within normal ranges of other thiosemicarbazone derivatives. The hydrogen atoms were all located in a different map, but those bonded to carbon were repositioned geographically. The hydrogen atoms were initially refined with soft restrains on the bond lengths and angles to regularize their geometry (C-H in the range 0.93-0.98 and N-H=0.87 Å) and with $U_{iso}(H)$ in the range 1.2-1.5 times U_{eq} of the parent atom, after which the positions were refined with riding constrains except the Hydrogen on Nitrogen which were allowed to refine freely [58]. Significant hydrogen bonding interactions are listed in table 2.

Fig. 2: Structure of AntCy with labelling of selected atoms. Anisotropic displacement ellipsoids exhibit 30% probability levels. Hydrogen atoms are drawn as circles with small radii.

Table 2. Selected bond length, bond angle and dihedral angles of AntCy

3.2 Colorimetric analysis and UV-Visible spectral studies:

The spectroscopic investigations of AntCy ($1x10^{-5}$ M) was carried out in DMSO as a solvent, AntCy showed broad absorption bands centred at 260, 312 and 403 nm which are attributed to π- π* and n- π* transitions. The interaction of AntCy with various anions (F^-, Cl^-, I^-, Br^-, OH^-, AcO^-, CN^-, ClO_4^-, HSO_4^- and $H_2PO_4^-$) and cations (such as Cr^{3+}, Mn^{2+}, Fe^{2+}, Fe^{3+}, Co^{2+}, Ni^{2+}, Cu^{2+} and Zn^{2+}) were investigated through colorimetric and UV-Vis spectral analysis. No change in the spectra was observed for other anions, except fluoride and for cations except cupric ion. Upon the addition of fluoride, a new band appeared with a bathochromic shift at 480 nm imparting an immediate orange colour from the colourless solution. To further quantification of the sensing, titrations were carried out with the addition of 20 equivalent of fluoride solution to the 1 x 10^{-5} M receptor. The spectral profile recorded thus is given in supporting data S7. Excess addition of fluoride results a hyperchromic shift along with isosbestic points of this red shifted π-π* band at 480 nm. This indicates the deprotonation of receptor and an increase in the conjugation of the system. The n-π* transition bands also show a bathochromic shift, which is due to the strong hydrogen-bonding interactions between the fluoride ion with receptor compound [15,56]. While the addition of

copper ion to the AntCy results the formation of a broad band in the range of 298 nm with high absorbance. A defined isobistic point was found at 383 nm, which attributes the multi-complex formation of AntCy-Cu. The UV-vis titration graph of fluoride and copper are as shown in Fig 4.

Fig. 3: UV Vis spectra of receptor AntCy with fluoride ion
UV Vis spectra of receptor AntCy with copper ion
Fig. 4: Benesi-Hildebrand and Job's plot of AntCy with fluoride and copper ions

Job's plot method was used to determine the stoichiometry ratio of the compound to the fluoride ion and copper ion, which give the receptor bind with fluoride ion in 1:1 ratio, and 2:1 for copper ion. The binding constant was calculated using Benesi-Hildebrand equation [57] which is as below,

$$\frac{1}{A-A_0} = \frac{1}{A_\infty - A_0}\left[\frac{1}{K[C]}+1\right]$$

Where, 'A, A_0 and A_∞' is the absorbance with a specific fluoride concentration, free compound and excess amount of ion respectively. 'K' is the association constant, and 'C' is the concentration of fluoride or copper ion added. The plot of 1/[C] Vs 1/(A -A_0) shows (Fig. 5) a linear relationship (R = 0.98). The association constant (K) was calculated by the ratio of intercept/slope and which got as 1.329×10^6 and 4.58×10^6 M^{-1} for fluoride and copper respectively. From the binding constant value, it is clear that the AntCy bind stronger towards copper ion than fluoride ion.

3.3 Fluorescence spectral studies

To know the selectivity of the receptor, fluorescence measurements were carried out with 10 equivalent of different anions (such as F^-, Cl^-, I^-, Br^-, OH^-, AcO^-, ClO_4^-, HSO_4^- and $H_2PO_4^-$) and cations (such as Cr^{3+}, Mn^{2+}, Fe^{2+}, Fe^{3+}, Co^{2+}, Ni^{2+}, Cu^{2+} and Zn^{2+}) with 1×10^{-5} M concentration of AntCy (S8). AntCy shows high emission intensity at 455 nm, when it excited at 400 nm. The addition of fluoride anion cause quenching of the emission with a blue shift. However, the addition of copper ion to AntCy results the enhancement of emission intensity at 455 nm, whereas no noticeable emission was observed with other cations. Further, while increasing the copper ion concentration, the emission intensity also increased. The observed enhancement in emission may be attributed due to the formation of new geometrically restricted five membered ring. Upon the addition of copper ion, the conformational restriction occurs due to delocalization of the charge created with in the molecule.

To confirm the stoichiometric ratio of receptor and fluoride, Job's plot were drawn in between [C]/([C]+[R]) Vs I_0/I, where [C], [R], I_0 and I are the concentration of fluoride or copper ion, concentration of receptor, intensity of free receptor and intensity with addition of ions respectively. It reveal the binding ratio between the receptor with fluoride and copper ion were 1:1 and 2:1 respectively. The fluorescence was quenched as disturbing the conjugation behaviour of receptor AntCy. The detailed spectra and graph as shown in Fig. 5 and 6.

Fig. 5 : (a) Emission Spectra of AntCy with fluoride anions
(b) Emission Spectra of AntCy with copper cations

Fig. 6 : Job's Plot for complexation of AntCy with fluoride and copper ions

3.4 Electrochemical analysis

The Fig 7 shows the behaviour of AntCy with fluoride and copper ion via electron transfer intercalation. The receptor shows less current density at 0.35mV, while adding the fluoride ion the current density increases with a voltage shift. Upon the addition of copper ion to the AntCy, a new reduction peak was observed at 0.61 V, where the current density was increased with increasing the concentration of copper ion. The newly formed peak corresponds to the $Cu^{2+/}Cu^{+}$ [61] reduction. The isosbestic points were found in both oxidative curve and reductive curve at 0.50 and 0.40 V respectively. Based on the increase in peak current of compounds by the addition of different concentration of fluoride ion, the binding constants, K_b were calculated according to the following equation,

$$i_p^2 = \frac{1}{K_b[C]}\left(i_{p_0}^2 - i_p^2\right) + i_{p_0}^2 - [C]$$

Where K_b is the binding constant, i_p and i_{po} are the peak currents with and without ion. A plot i_p^2 v/s. $\frac{(i_{p_0}^2 - i_p^2)}{[C]}$ gave a straight line, and the binding constants of the receptor with fluoride and copper ions were calculated as 0.270 x 10^6 and 11.63 x 10^6 M^{-1} respectively, where AntCy with copper ion have more association constant than with fluoride ion, corroborated to the same tendency of UV-Vis spectra calculations. From the binding constant value, the Gibbs free energy for the sensing processes was calculated using the equation, $\Delta G = - RT \ln K_b$, and was found to be -30.98 and -28.14 KJ mol^{-1} for fluoride and copper respectively. The negative value shows the spontaneity of the sensing process.

Fig. 7: (a) CV of receptor AntCy with fluoride ion
(b) CV of receptor AntCy with copper ion

Fig. 8: Binding energy graph of receptors AntCy for (a) fluoride ion and (b) copper ion

3.5 ^{1}H NMR titration studies

To investigate the molecular interaction between receptors and fluoride anion, ^{1}H NMR titration study in DMSO-D_6 solvent were done with receptors AntCy in presence and absence of fluoride anion. The ^{1}H spectra shows a singlet at δ=11.55 and 9.30 ppm for the N-H protons nearby the anthracene moiety and cyclohexyl group respectively. Upon the addition, of fluoride intensity of the signals started decreasing eventually with the disappearance of the peaks with the excess addition. With 3 equivalents of fluoride addition two new peaks started appearing at δ 7.60 and 6.88. This indicates the interaction of F···H···N protons. Excess fluoride aids the deprotonation of the moiety. The multiplet at 4.23 ppm belonging for the N-C-H cyclohexyl proton. This signal also undergoes significant reduction in the presence of fluoride ion. This peak also found to disappear completely with the excess addition of fluoride. This may be due to the effect of conjugation in the deprotonated species.

Fig. 9: ^{1}H NMR titration data of AntCy with F^-

3.6 Computational studies

3.6.1 Geometry Optimization

The differences in geometries between S_0 and S_1 states and fluorescence spectra for Chemosensor (AntCy), fluoride ion complex (AntCy-F) and copper complex (AntCy-Cu) have been investigated in detail after the geometry optimization. The ground state (S_0) and excited state (S_1) structures of the receptors have been optimised, and corresponding frequencies were calculated. The ground state and excited state SCF energy of AntCy (S_{A0}) is -8.87×10^5 and -8.86×10^5 Kcal/mol respectively. In the ground state, the cyclohexyl group and anthracene moiety are not coplanar. The dihedral angle between anthracene moiety and thionyl group is 28.89^0 and the dihedral angle between boat formed cyclohexane group and semicarbazone moiety is 40.74^0. A subsequent vibrational frequency analysis further confirmed that the structure are at a global minima. The ground state optimised spatial coordinates and IR frequencies were given in the supporting documents. The ground state optimised energy of AntCy-F complex is less than that of AntCy, which comes around -9.46×10^5 Kcal/mol. In the ground state of AntCy, the angle between anthracene moiety and semicarbazone groups are at 120^0 and the dihedral angle between cyclohexyl group and se micarbazone moiety is 36^0.

In the excited state (S_{A1}) of AntCy, the dihedral angle between cyclohexane group and thiosemicarbazone group is 93.91^0 and the same for anthracene moiety and thionyl group is 27.47^0. But, after bonding with fluoride ion, the dihedral angles twisted to 177^0 for cyclohexyl-thiosemicarbazone group and 14^0 for anthracene-thionyl group. The thiocarbonyl group (C=S) bond distance remains same in both states. The photoirradiation makes the nearly planar structure of H1-N-C-N in ground state (0.01^0 Dihedral angle) twist to 176^0 for the receptor excited structure. For the ground state structure of the complex (AntCy-F), the same dihedral angle is 0.5^0 and for the excited state it is twist to 177^0 and destroying their planarity. The bond distance between N1-H1 in receptor's ground state optimised structure and excited structure are almost equal (nearly 1.02 Å). The AntCy shows same N2-H2 bond distance in ground and excited state and even after the formation of fluoride complex. In excited state, the hydrogen bond is only between H1 which was more than that of ground state (0.999 Å). From this it is clear that the hydrogen is removed from N25, which is nearby anthracene moiety and not from the N27 which is nearby cyclohexyl group and the removal of the hydrogen takes place at the excited state. Whereas in the case of AntCy-Cu complex, the Cu-S and Cu-N bond distance are 2.41 and 2.06 Å respectively. The C=S bond distance found to be 1.78 Å, which is 1.60 Å in AntCy., which attributes the bond between 'C' and 'S' is elongated during complexation. The dominant structural parameters in the optimised structures before and after sensing is listed in Table 3. There is no notable change in bond parameters at ground state and excited state. Which attributes the binding was takes place at the ground state. As the speculation on the decreased distance between Fluoride ion and upper proton H1 and increased distance between Fluoride ion and H2 in S1 state, the intermolecular excited-state proton transfer (ESPT) will take place in S1 state in the presence of fluoride anion. From this it concluded that the binding energy of the fluoride ion to H1 hydrogen is more than of H2.

Fig. 10: (a) Ground state and (b) Excited state structure of AntCy with fluoride
Table 3: Bond characters of AntCy, AntCy-F and AntCy-Cu at ground state and excited state

3.6.2 UV–Vis spectra and molecular orbital analysis:

In order to investigate the absorption behaviour of AntCy in sensing of fluoride, molecular excitation study was carried out. AntCy shows (as shown in S8) an intense absorption at 366 nm with 0.2108 oscillating strength as a dominant $\pi \rightarrow \pi*$ type transition, which is from the highest occupied molecular orbital (HOMO, 96) to the lowest unoccupied molecular orbital (LUMO, 97). The local HOMO electron is delocalized through anthracene moiety, carbazonyl and cyclohexyl groups. In the local transition, this delocalized electrons (HOMO) were transited to only anthracene moiety (LUMO). The second dominant transition also follows same root, which is at 265 nm wavelength and the transition is from second highest occupied molecular orbital (HOMO-1) to LUMO with 3.48 eV energy gap. Another less energy transition, HOMO-2 to LUMO, was in between carbazyl group and anthracene moiety.

The absorption wave length for strongest $\pi \rightarrow \pi*$ transition is shifted in to 373 nm for receptor-fluoride complex, where the transition from HOMO(101) to LUMO(102) orbitals, which is in between carbonyl group and anthracene moiety. The other main transitions are H-1→L and H-2→L. In the HOMO-1, the electron delocalized on anthracene, cyclohexyl and carbazone groups. But, in HOMO-2 orbital, the electrons are located on carbazonyl and cyclohexyl group not in the anthracene moiety. In the case of AntCy-Cu complex, the excitation wavelength at 409 nm, which was very closer to the experimental value. The transition with high oscillating strength is at 523 nm, where the transition is between HOMO-3 to LUMO. The other major transitions are at 571 nm, where the transition is between HOMO to LUMO with 22 % abundance. Fig 11 shows all the major electronic transitions before and after sensing respectively.

The mulliken charge analysis was done for the further clarification of ESPT process. For this, the ground state and excited state mulliken charges of complexes were compared. By comparing the mulliken atomic charge on N(25) and N(27) at ground state and excited state, the excited state N(25) had high increase than N(27). This further confirms that the Hydrogen removal was at N(25). In the ground state of AntCy-F complex, the charges on N(25), H(31) and Fluoride were -0.1518, 0.1347 and -0.6149 e respectively. The photo-excitation can induces large influence in the charges for the three atoms, and it seen as -0.3088, 0.2623 and -0.3638 e in excited state corresponding N(25), H(31) and F respectively. This result supported the ESPT process such a way that, in the excited state movement of the proton from nitrogen atom to fluoride anion.

Fig. 11: The major molecular orbitals contributed to the transition for AntCy and AntCy-F
Table 4. Absorption details of receptor AntCy, AntCy-F and AntCy-Cu complexes

3.6.3 Transition state, IRC and Gibbs free energy calculations

In order to capture the dynamics feature of the hydrogen transfer reaction, the profile of Gibb's free energy in solution for the sensing mechanism is calculated. The ground state Gibb's free energy of the AntCy was found to be -8.86×10^5 Kcal/mol. The formation of

transition state, the complex between Fluoride and receptor AntCy is endergonic by 239.81 Kcal/mol. In the intermediate and transition state complexes, the fluoride anion was interact with receptor's carbazonyl hydrogen, through hydrogen bonding. Intrinsic Reaction Coordination (**IRC**) calculation, for the optimised structure of the TS, to verify the correct transition state connecting the minima of the reactants and products of interest of transition state was performed. Relaxation of transition state towards the products by IRC calculations detect an intermediate which was further confirmed with frequency calculation. The Gibbs free energy profile of the mechanism was as shown in the Fig. 12.

The total change in Gibbs free energy in the reactions are 174.01 Kcal/mol. The less Gibbs free energy difference in between reactant and product says that the reaction was in reversible, and best supporting for the explanation of Chemosensing mechanism. The calculated entropic change ($\Delta s = \frac{\Delta H - \Delta G}{T}$) in the formation process of the hydrogen bridge involving fluoride ion is -0.0435 KJ/mol, which indicates that the formation process of the hydrogen bonded complex is thermodynamically allowed. The binding constant of the fluoride was calculated from the Gibbs free energy value [$\ln(Ka) = \frac{-\Delta G}{RT}$] which was found at 1.45×10^5 M^{-1} which was close to experimental value.

Fig 12: Gibbs free energy profiles for the Receptor AntCy- F sensing mechanism. R: reactant; IM: intermediate; TS: transition state; P: product. All Gibbs free energies are in kcal mol^{-1}; all bond lengths are in Å

3.6.4 Emission spectral studies

The emission spectra were calculated by the TD-DFT/B3LYP method. There are two paths when S_1 state relaxes to S_0 state corresponding to the excited process, the spectra as shown in supplementary data S9. In AntCy, The single electron in 97^{th} orbital (LUMO), descends to the single occupied molecular orbital (SOMO) of 96^{th} orbital, where there are large overlap of the electrons over anthracene segment. There the emission wavelength falls on 468 nm with a less energy gap (2.64 eV) and maximum oscillating strength (0.366). Another major emission transition is seen at 325 nm, in which the electron emitted from LUMO+1 to HOMO, and the electrons in these two orbitals present almost overlap over the anthracene moiety and one side of carbazonyl groups. The formation of the intra-molecular hydrogen bond with fluoride ion induces the fluorescence spectra by 229 nm. The oscillating strengths of receptor and complex were 0.366 and 0.2552 respectively. The excitation energy of the receptor's excitation and emission energies are -38453.14 eV and -38450.81 eV respectively. For AntCy-Cu complex, the emission with higher oscillating strength was at 563 nm with 2.19 eV energy, which was from LUMO to HOMO orbital transition. Other major transition at this wavelength was from LUMO to HOMO-1 orbital. The energy for the emission process is -1251.86 eV. The fluorescence quenching effect is matching with experimental values and theoretical predictions. The detailed emission values were tabled (Table 5).

Table 5: The fluorescence emissions for the receptors AntCy and AntCy-F

3.6.5 Potential energy curves (PES)

To reveal the more features of ESPT process in the S_1 state for the fluoride-complex, the potential-energy surface (PES) of ground state and excited state had been calculated with only by varying N25–H38 bond length from 0.90 to 1.80 Å in steps of 0.05 Å, which can provide qualitative energetic pathways for the ESIPT process. The energy of excited state and ground state were decreased when increasing N-H bond length and it increases through a stable point at the bond length 1.00 Å and the same was for ground state is 1.15 Å, which are just the stable optimized geometry of S_1 and S_0 states. From this data it is clear that the fluoride anion prefer to form an intermolecular hydrogen bond where the hydrogen transferred from nitrogen (N2) to fluoride ion. Thus the sensing mechanism was of the receptor was first react with added fluoride ion and forms hydrogen bond, not in free H^+ ion. Hence it had the red shift in its fluorescence emission spectra and UV absorption spectra and the fluorescence colour signal directly detect with the naked eye. The potential energy graph for the AntCy-F complex with varying N(25)-H(38) at both ground state and excited state were given in the Fig 13.

Fig 13: Potential-energy curves of excited state (S1) and ground state for complex A–F, which is the function of the N25– H42 bond length and corresponding N(27)-H(43) bond length

3.6.6 NBO analysis

NBO method gives information about interactions in both filled and virtual orbital spaces that could enhance the analysis of intra- and inter-molecular interactions. The change in bond length between N2–H2 and H2-F of optimised geometries in S_0 and S_1 states and the emission studies predicts that the proton nearby anthracene moiety has a preference for fluoride than the N4 proton nearby cyclohexyl group for both reversible binding, which takes place in S_1 state via excited state proton transfer (ESPT) process. In order to support this data, the calculation of binding energy between two kinds of binding sites of F-H and the residue for fluoride complex were calculated.. The binding energies ΔE can be calculated as $\Delta E = E_{AB} - (E_A+E_B)+BSSE$, where BSSE is the Basis Set Superposition Error, E_A and E_B are the energies for the fragments A and B localized in the compound AB. For the fluoride complex, the binding energies between the two segments were separated as H1-F and H2-F and calculated [32].

Picturesque the priority of proton, which is near to anthracene moiety, in attaching to Fluoride ion, the natural bond orbital (NBO) analysis for ground state and excited state fluoride complex compounds have been performed. NBO analysis provides the most accurate possible 'natural Lewis structure' picture, because all orbital details are mathematically chosen to include the highest possible percentage of the electron density. The receptor AntCy-F, the N1-H1 and N2-H2 bonds in the S_0 state is one single σ bond with the Wiberg Bond Index (WBI) are 0.61 and 0.5 respectively. And the same for fluoride and hydrogen is much lower and corresponding bonding character shows there is no chemical bonds between F and H atoms in S_0 state. The natural atomic hybrids where calculated by giving the percentage of the NBO on each hybrid atoms. The single bond hybridisation in between N25-H1 and N27-H2 were found. In excited structure, the N25-H32 bond was vanished, it shows there is no N1-H1 bond in excited state. In ground state sp^2 Nitrogen was hybridised to s Hydrogen and it vanish at excited state. Due to this, the strong donor–acceptor interaction

between fluoride and the AntCy can be treated by the second-perturbation energy E(2) which has been calculated from electron donor orbital, acceptor orbital and the interacting stabilization energy at ground state and excited state and using this we can be explain the weak interaction [52]. The second order perturbation equation as below,

$$E(2) = \Delta E = \frac{q_i F_{ij}^2}{\varepsilon_j - \varepsilon_i}$$

Where E(2) is the second perturbation energy, F_{ij} is the off-diagonal element in the NBO Fock matrix, q_i is the donor orbital occupancy, and εi and εj are orbital energies. There were two type of interaction σ -σ* and n-σ*, in between N25 – H32 and N27 – H31 towards Fluoride ion at ground state. But in excited state the N25-H32 bond vanishes and only shows N27 –H31 with fluoride ion. The second order perturbation energy varies from 59 to 0.1 Kcal/mol and 29 to 1 Kcal/mol for N25-H32 and N27-H31 towards F(50) respectively. All weak interactions have generated from lone-pair electron (n) and core pair electron (σ) of F, in which the LP F(50) → BD*(1) N25–H32 pairs induce larger interaction with fluorine atom rather than LP F(50) → BD*(1) N27-H31 pairs. In the case of AntCy-Cu complex, the nitrogen and sulphur atoms act as donor and copper ion act as acceptor. The highest second order energy was shown the transition between LP N(24) → LP* Cu(50), where the energy is 24.35 Kcal/mol, and n → n* transition, the non-bonding electron of nitrogen to non-bonding electron of copper ion. The higher second order perturbation energy transition of S(29) to Cu(50) is n → σ* transition, where the non-bonding electron of sulphur to core pair electron of copper atom.

The highest second order perturbation energy at excited state is LP F(50) → LP* H 32 with the energy of 356.30 Kcal/mol where the interaction generated from lone pair electron n of Fluoride to n* of hydrogen. The weak interaction of N25 towards H32 is core pair electron of Nitrogen to Hydrogen's lone pair electron, which is less energy than fluorine-hydrogen interactions. The NBO characters in ground state and excited state were given in the table 6. The large overlap of the electron density for the interaction confirms the strong donor–acceptor interaction, indicating the H32 protons prefer to interact with Fluoride ion rather than N25. The weak interaction in complex a-F is assigned from lone-pair electron n of F or N2 atoms to n* of H2, well illuminating that the proton at neighbouring anthracene moiety (H2) tends to transfer to F and forms N···H···F strong hydrogen bond. The tables were listed in supplementary data S11 and S12.

Table 6: Second perturbation energy of donor- acceptor interaction at ground and excited states of AntCy-F complex

4. Sensing mechanism

From the experimental excitation spectra the fluorescence quenching of the chemosensor AntCy, due to the presence of fluoride ion is evident. Where as in the presence of copper ion, the fluorescence enhancement was takes place. From the NMR titration, the dehydrogenation takes place at N(25), which was nearby the anthracene moiety. But, the excess addition of fluoride ion will cause the removal of both N-H protons and for a hydrogen bonded fluoride complex. The proton transfer takes place at the excited state of receptor-fluoride complex, which was confirmed with NBO analysis and potential energy

surface study. While the electronic excitation transition from occupied orbital to unoccupied orbitals, more possible and allowed transition are to delocalised electron in Anthracene moiety. This infer that the anthracene moiety plays an important role to provide binding site of fluoride ion. While, the copper binding was happened at ground state with intermolecular charge transfer (ICT).

Fig 14: The Fluorescence sensing binding mode and mechanism of receptors

Acknowledgment

SMB is thankful for the financial support from the MHRD (India) and Endeavour Research Fellowship (Australia). Special thanks to Prof. Rob Stranger to give the access to the supercomputer facilities of the National Computational Infrastructure.

Reference:

1. K.R. Dey, B.M. Wong, M.A. Hossain, Tetrahedron Lett., 51 (2010) 1329-1332
2. Y. Qu, J. Hua, H. Tian, Org. lett., 12 (2010) 3320-3323
3. H.W. Rhee, J.C. So, H.Y. Sang, O.J. Yong, H.P. Hun, R.M. Pinto, J.C. Cameselle, F.J. Sandoval, S. Roje, K. Han, D.S. Chung, J. Suh, J.I. Hong, J. Am. Chem. Soc., 131 (2009) 10107-10112
4. R. Jun, W. Sun, Science China., 55 (2012) 1428-1434
5. M. Cametti, K. Rissanen, Chem. Commun., 20 (2009) 2809-2829
6. S.W. Zhang, T.M. Swager, J. Am. Chem. Soc., 125 (2003) 3420-3421
7. G.Y. Li, G.J. Zhao, Y.H. Liu, K.L Han, G.Z He, J. Comput. Chem., 31 (2010) 1759–1765
8. C.B. Black, B. Andrioletti, A.C. Try, C. Ruiperez, J.L. Sessler, J. Am. Chem. Soc., 121 (1999) 10438–10439
9. S.K. Kim and J. Yoon, Chem. Commun., (2002) 770–771.
10. H.T. Chifotides, B.L. Schottel and K.R. Dunbar, Angew. Chem. Int. Ed., 49 (2010) 7202–7207
11. P. Song, J. X. Ding, T. S. Chu, Spectrochim. Acta, Part A, 97 (2012) 746–752
12. S. Dalapati, M. A. Alam, S. Jana, N. Guchhait, J. Fluorine Chem., 132 (2011) 536-540
13. P. Bose, P. Ghosh, Chem. Comm., 46 (2010) 2962-2964
14. S. Guha, S. Saha, J. Am. Chem. Soc., 132 (2010) 17674-17677
15. M. Bonizzoni, L. Fabbrizzi, A. Taglietti, F. Tiengo, Eur. J. Org. Chem., 16 (2006) 3567-3574
16. T. Gunnlaugsson, A.P. Davis, J.E. O'Brien, M. Glynn, Org. Lett., 4 (2002) 2449–2452.
17. X. Zhang, Y.B. Wu, S.M. Ji, H.M. Guo, P. Song, K.L. Han, W.T. Wu, W.H. Wu, J. Org. Chem., 75 (2010) 2578–2588.
18. F. Han, L.N. Chi, X.F. Liang, S.M. Ji, S.S. Liu, F.K. Zhou, Y.B. Wu, K.L. Han, J.Z. Zhao, T.D. James, J. Org. Chem., 74 (2009) 1333–1336
19. G.Y. Li, G.J. Zhao, Han, K.L. Han, G.Z. He, J. Comput. Chem., 32 (2011) 668–674
20. G.Y. Li, T. Chu, Phys. Chem. Chem. Phys., 13 (2011) 20766–20771
21. Q. Wang, Y. Xie, Y. Ding, X. Li, W. Zhu, Chem. Comm., 46 (2010) 3669-3671
22. P. D. Beer, Acc. Chem. Res., 31 (1998) 71-80

23. F. Weigend, R. Ahlrichs, Phys. Chem. Chem. Phys., 7 (2005) 3297-305.
24. X. F. Yang, H. P. Qi, L. P. Wang, Z. Su, G. Wang, Talanta, 80 (2009) 92-97
25. R. Hu, J. A. Feng, D. H. Hu, S. Q. Wang, S. Y. Li, Y. Li, G. Q. Yang, Angew. Chem., Int. Ed., 49 (2010) 4915-4918
26. F. Wang, J. Wu, X. Zhuang, W. Zhang, W. Liu, P. Wang, S. Wu, Sens. Actuators. B., 146 (2010) 260-
27. J. S. Chen, P. W. Zhou, L. Zhao, T. S. Chu, RSC Adv., 4 (2014) 254-259
28. M.E. Huston, E.U. Akkaya, A.W Czamik, J. Am. Chem. Soc., 23 (1989) 8735-8737
29. T. Ueno, Y. Urano, K. Setsukinai, H. Takakusa, H. Kojima, K. Kikuchi, K. Ohkubo, S. Fukuzumi, T. Nagano, J. Am. Chem. Soc., 126 (2004) 14079–14085
30. P. Das, A. Ghosh, H. Bhatt, A. Das, RSC Adv., 2 (2012) 3714–3721
31. J.S. Chen, P.W. Zhou, G.Y. Li, T.S. Chu, G.Z. He, J. Phys. Chem. B., 117 (2013) 5212−5221
32. G.Y. Li, G.J. Zhao, Y.H. Liu, K.L. Han, G.Z. He, J. Comput. Chem., 31 (2010) 1759-1765
33. K. Eichkorn, O. Treutler, H. Ohm, M. Haser, Chem. Phys. Lett., 1995, **240**, 283-290.
34. S.L.A. Kumar, M.R. Tamilarasan, M.S. Kumar, A. Sreekanth, Ind. Eng. Chem. Res., 50 (2011) 12379-83
35. S. L. A. Kumar, M.S. Kumar, R. P. John, P. T. Muthiah, Mater. Sci. Eng. C., 33 (2013) 2519-2525
36. M. S. Kumar, S.L.A. Kumar, A. Sreekanth, Mater. Sci. Eng. C., 33 (2013) 3346-3352
37. S.L.A. Kumar, M.S. Kumar, P.B. Sreeja, A. Sreekanth, Spectrochim. Acta Part A., 113 (2013) 123-129
38. M. E. Casida, C. Jamorski, K.C. Casida, D.R. Salahub, J. Chem. Phys., 108 (1998) 4439-4449.
39. R.E. Stratmann, G.E. Scuseria, M.J. Frisch, J. Chem. Phys., 109 (1998) 8218-24.
40. R. Bauernschmitt, R. Ahlrichs, Chem. Phys. Lett., 256 (1996) 454-64
41. C. Van Caillie, R. D. Amos, Chem. Phys. Lett., 308 (1999) 249-55.
42. B. I. Dunlap, J. Mol. Struct. (Theochem), 529 (2000) 37-40
43. J. P. Foster, F. Weinhold, J. Am. Chem. Soc., 102 (1980) 7211-7218.
44. S.K. Schneider, G.R. Julius, C. Loschen, H.G. Raubenheimer, G. Frenking, W.A. Herrmann, Dalton Trans., (2006) 1226-1233
45. T. Yanai, D. Tew, N. Handy, Chem. Phys. Lett., 393 (2004) 51-57
46. K. Eichkorn, O. Treutler, H. Ohm, M. Haser, R. Achlrichs, Chem. Phys. Lett., 240 (1995) 283-289
47. K. Eichkorn, F. Weigend, O. Treutler, R. Achlrichs, Chem, Acc., 97 (1997) 119-124
48. A. Schaefer, H. Horm, R. Ahlrichs, J. Chem. Phys., 97 (1992) 2571-2577
49. A. Schafer, C. Huber, R. Ahlrichs, J. Chem. Phys., 100 (1994) 5829–5835.
50. G. Zhao, K. Han, Comput. Chem., 29 (2008) 2010–2017
51. G. Zhao, K. Han, Y-B. Lei and Y-S. Dou, J. Chem. Phys., 127 (2007) 094307-1-094307-6
52. B. Miehlich, A. Savin, H. Stoll, H. Preuss, Chem. Phys. Lett., 157 (1989) 200–206
53. C. Peng, H.B. Schlegel, Israel J. of Chem., 33, (1993) 449

54. C. Peng, P.Y. Ayala, H.B. Schlegel, M.J. Frisch, J. Comp. Chem., 17 (1996) 49
55. A. Kovalchuk, J. L. Bricks, G. Reck, K. Rurack, B. Schulz, A. Szumna, H. Weibhoff, Chem. Commun. 2004, 1946-1947
56. B.C. Tzeng, Y.F. Chen, C.C. Wu, C.C. Hu, Y.T. Changa, C.K. Chena, New J. Chem., 31 (2007) 202
57. A. Sreekanth, H.K. Fun, M.R.P. Kurup, J. Mol. Struct., 737 (2005) 61–67
58. Brewer, G. J. Chem. Res. Toxicol. 23 (2010) 319.
59. Sparks, D. L.; Schreurs, B. G. Proc. Natl. Acad. Sci. U.S.A., 100 (2003) 11065.
60. Valko, M.; Morris, H.; Cronin, M. T. D. Curr. Med. Chem., 12 (2005) 1161.
61. Bruijn, L. I.; Miller, T. M.; Cleveland, D. W. Annu. Rev. Neurosci., 27 (2004) 723

Fig 1 Structure of AntCy

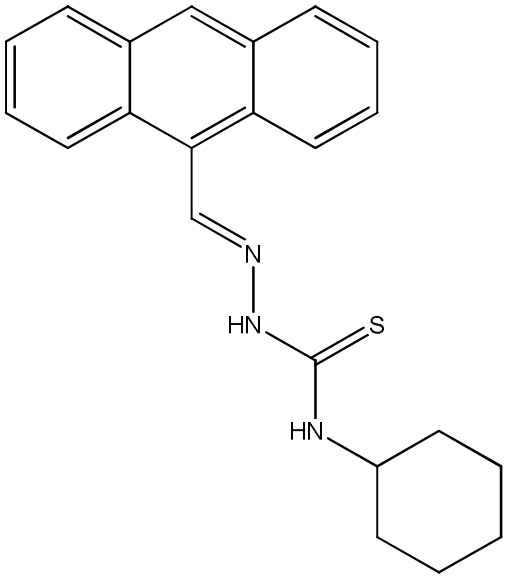

Fig 2. Fig. 2: Structure of AntCy with labelling of selected atoms. Anisotropic displacement ellipsoids exhibit 30% probability levels. Hydrogen atoms are drawn as circles with small radii.

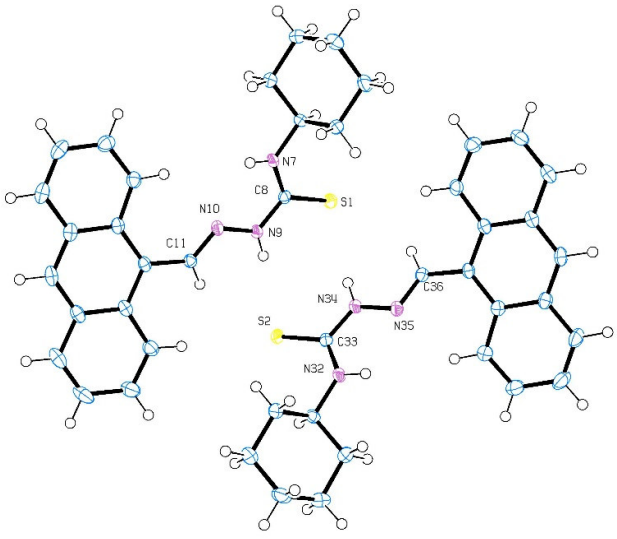

Fig. 3: UV Vis spectra of Receptor AntCy with different concentration of fluoride ion and copper ion

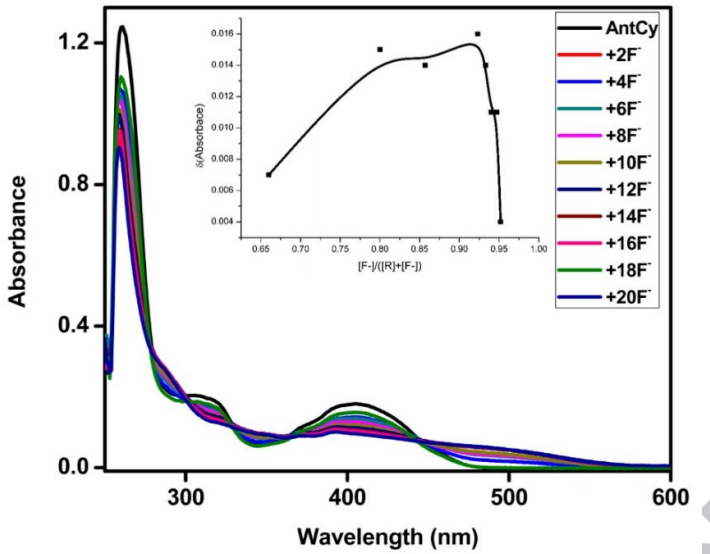

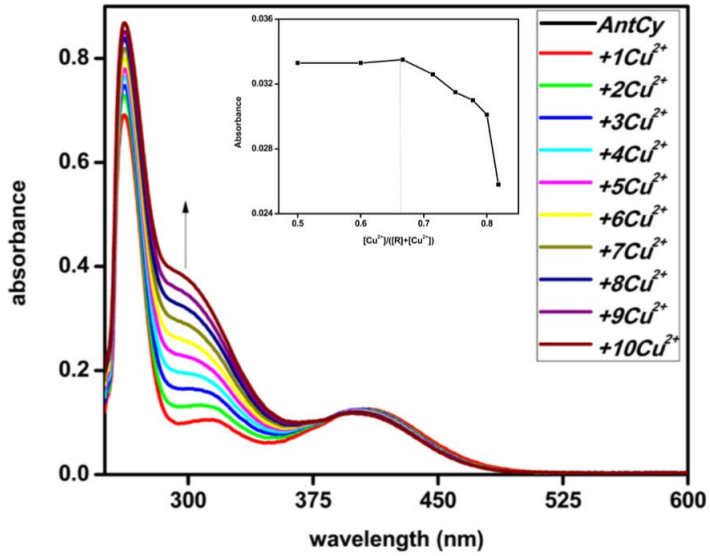

Fig. 4: Benesi-Hildebrand graph of receptor AntCy with (a) fluoride ion (b) copper ion

(a)

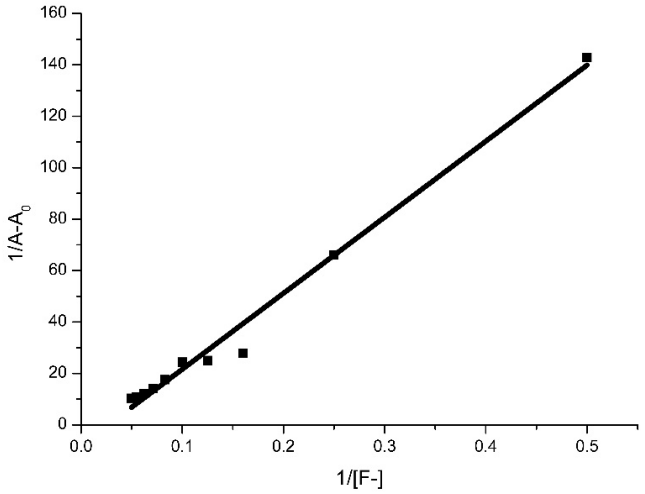

(b)

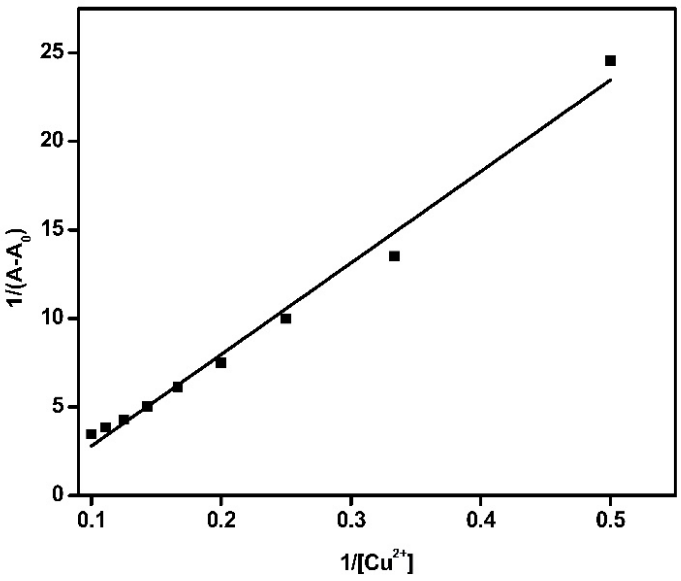

Fig. 5: Emission Spectra of receptor AntCy with (a) fluoride anions and (b) copper cation

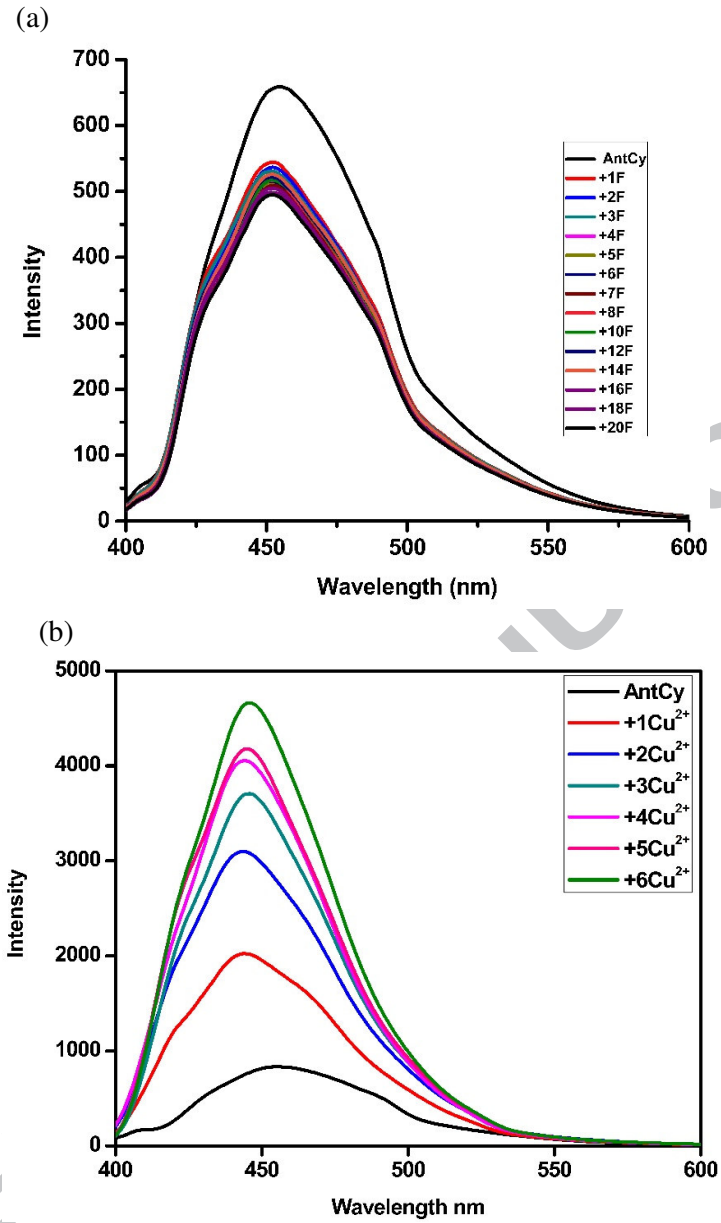

Fig. 6: Job's Plot for complexation of AntCy with (a) fluoride anion and (b) copper cation

(a)

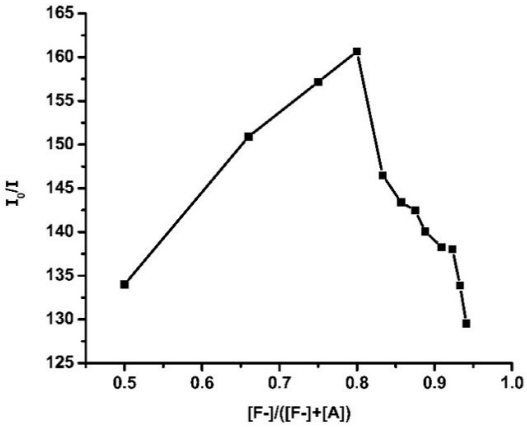

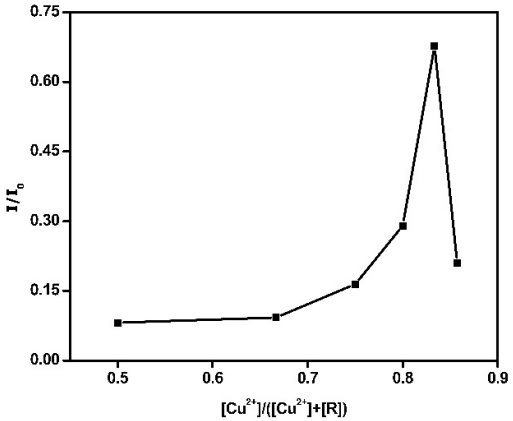

Fig. 7 : CV of Receptor AntCy with (a) fluoride ion and (b) copper ion

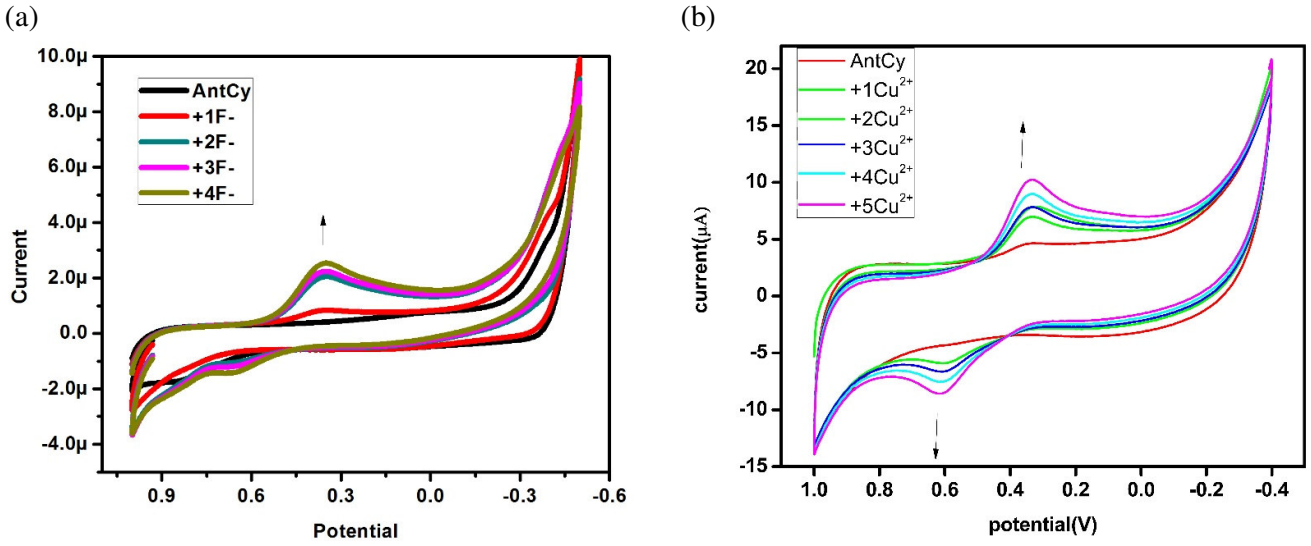

Fig. 8: Binding energy calculation graph of receptor AntCy with (a) fluoride and (b) copper using CV data

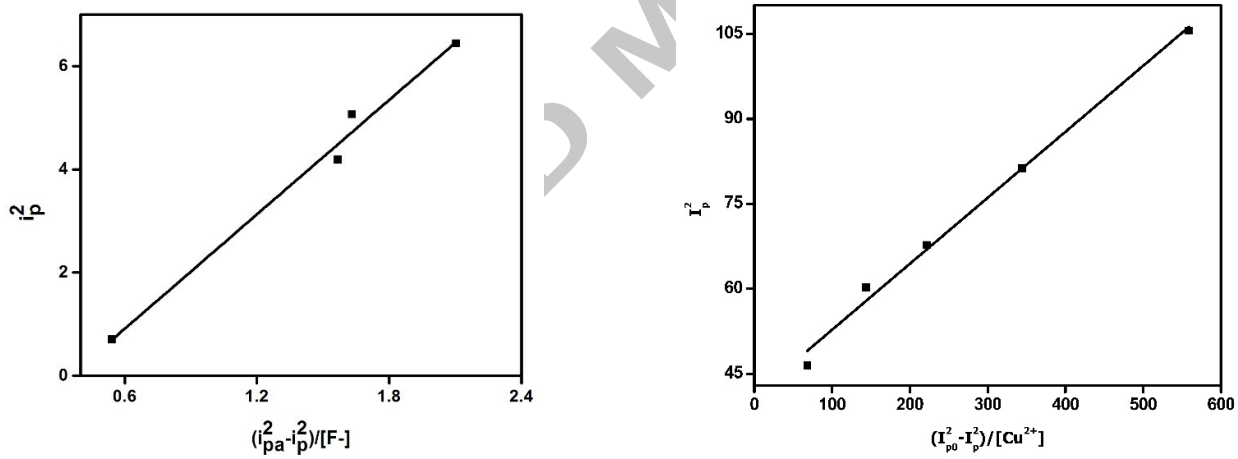

Fig. 9: ^{1}H NMR titration of AntCy with fluoride ion

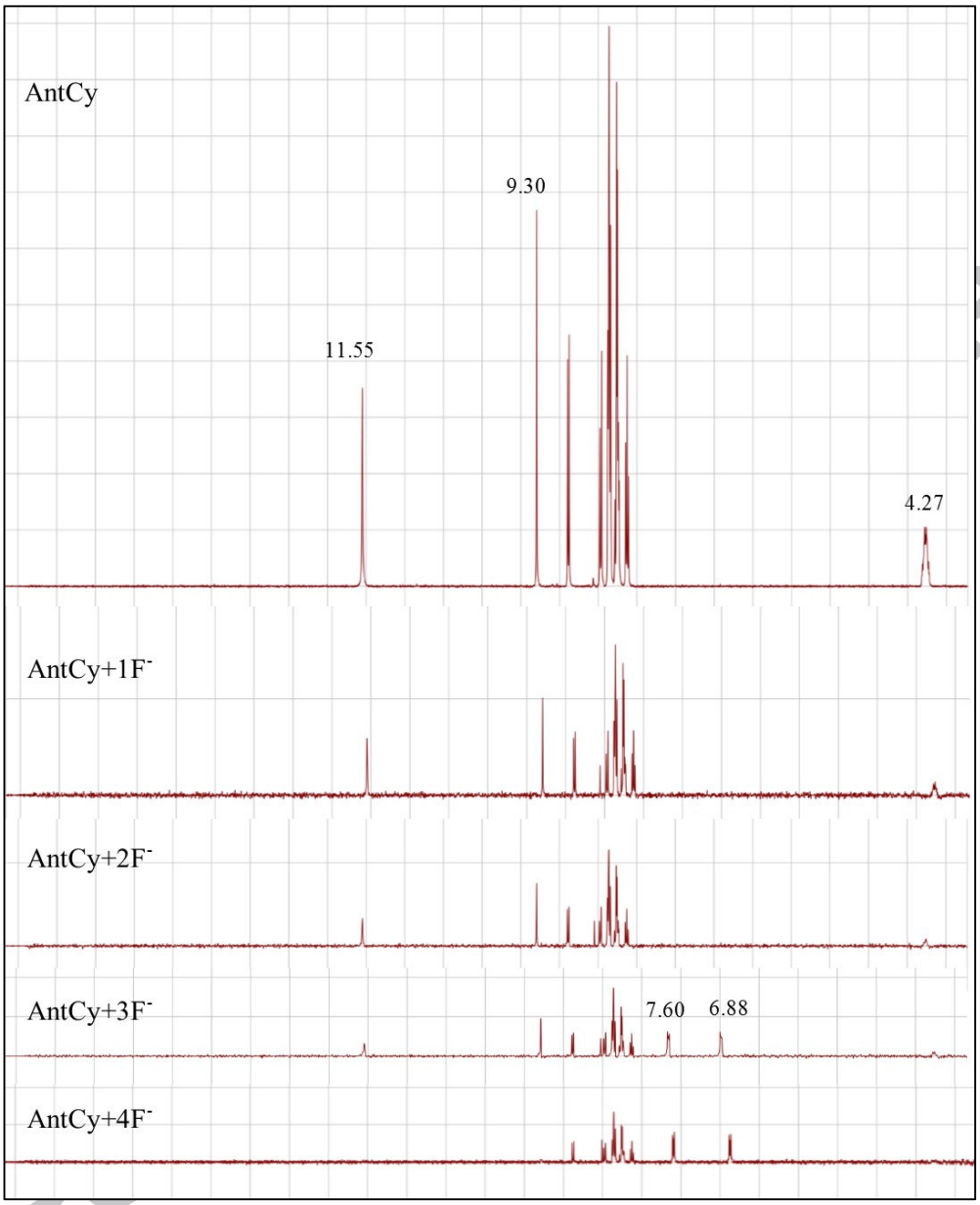

Fig. 10: Ground state and excited state structure of receptors with fluoride ion

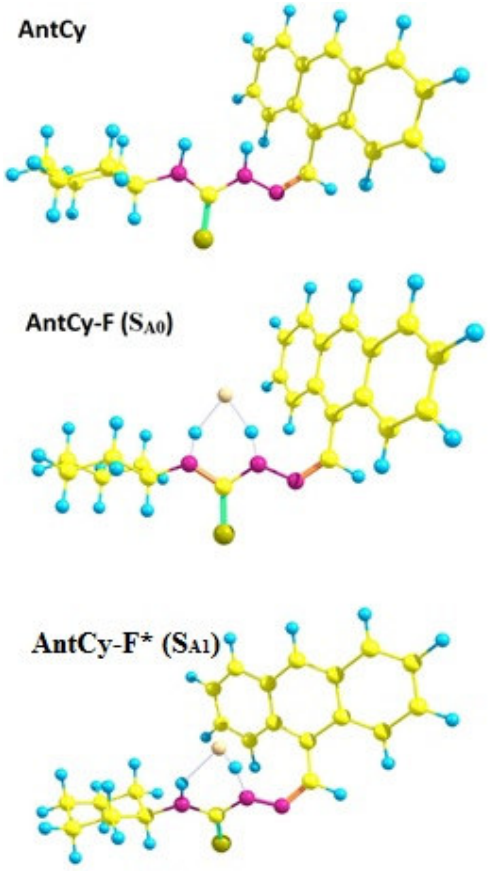

Fig 11: The major molecular orbitals contributed to the transition for AntCy and AntCy–F

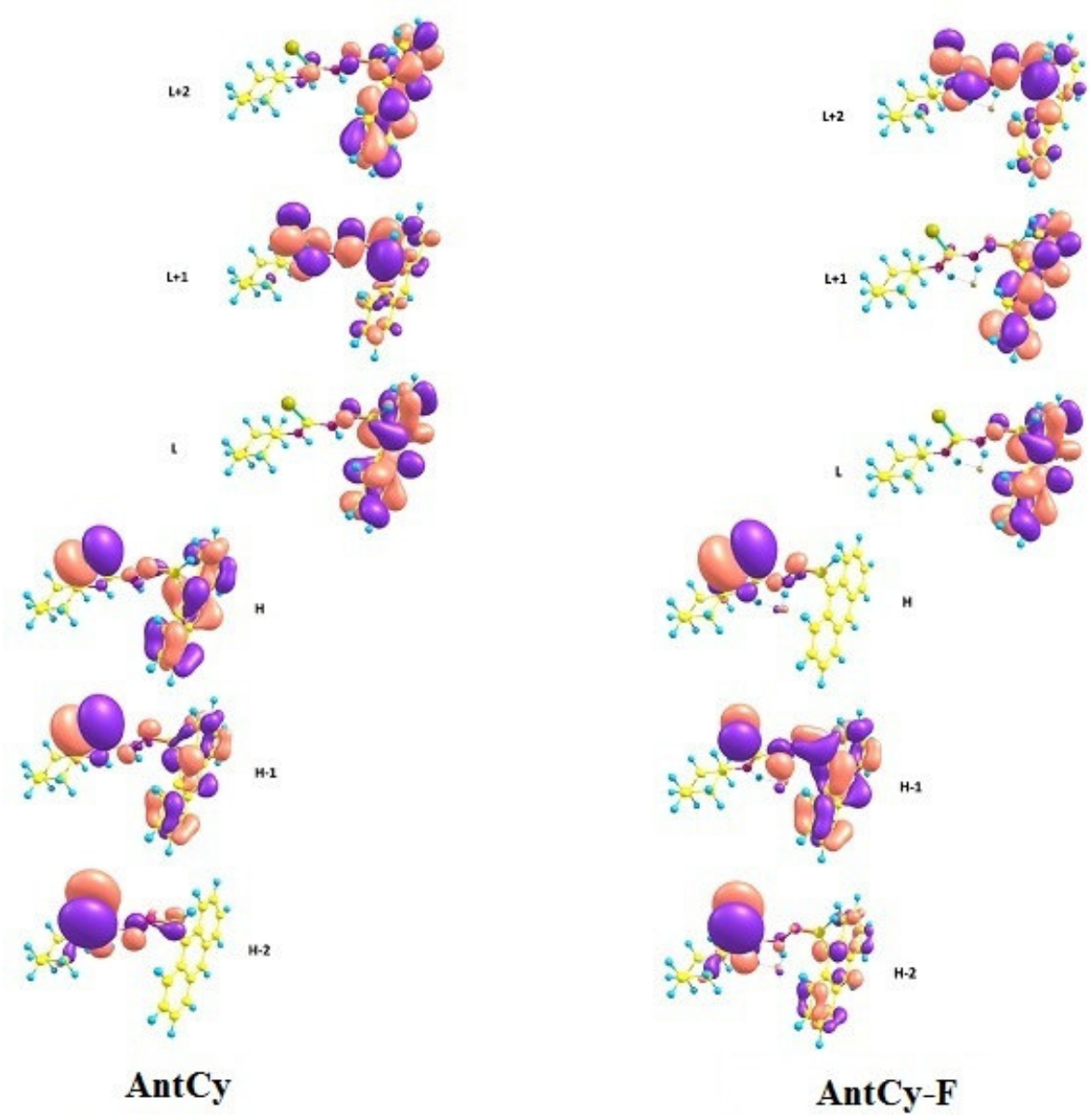

Fig 12: Gibbs free energy profiles for the Receptor AntCy- Fluoride sensing mechanism. R: reactant; IM: intermediate; TS: transition state; P: product. All Gibbs free energies are in kcal mol^{-1}; all bond lengths are in Å

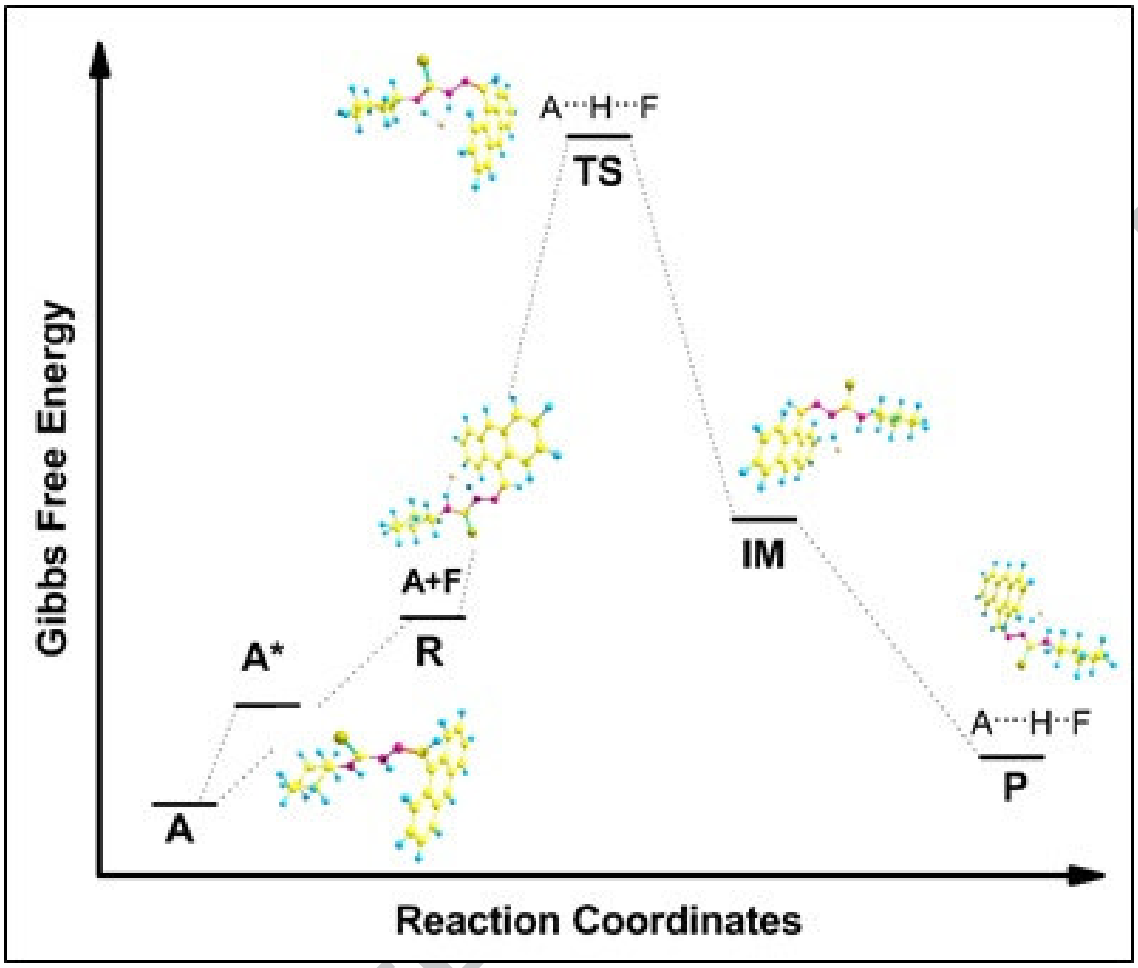

Fig 13: Potential-energy curves of excited state (S1) and ground state for complex AntCy–F, which is the function of the N25– H42 bond length and corresponding N(27)-H(43) bond length

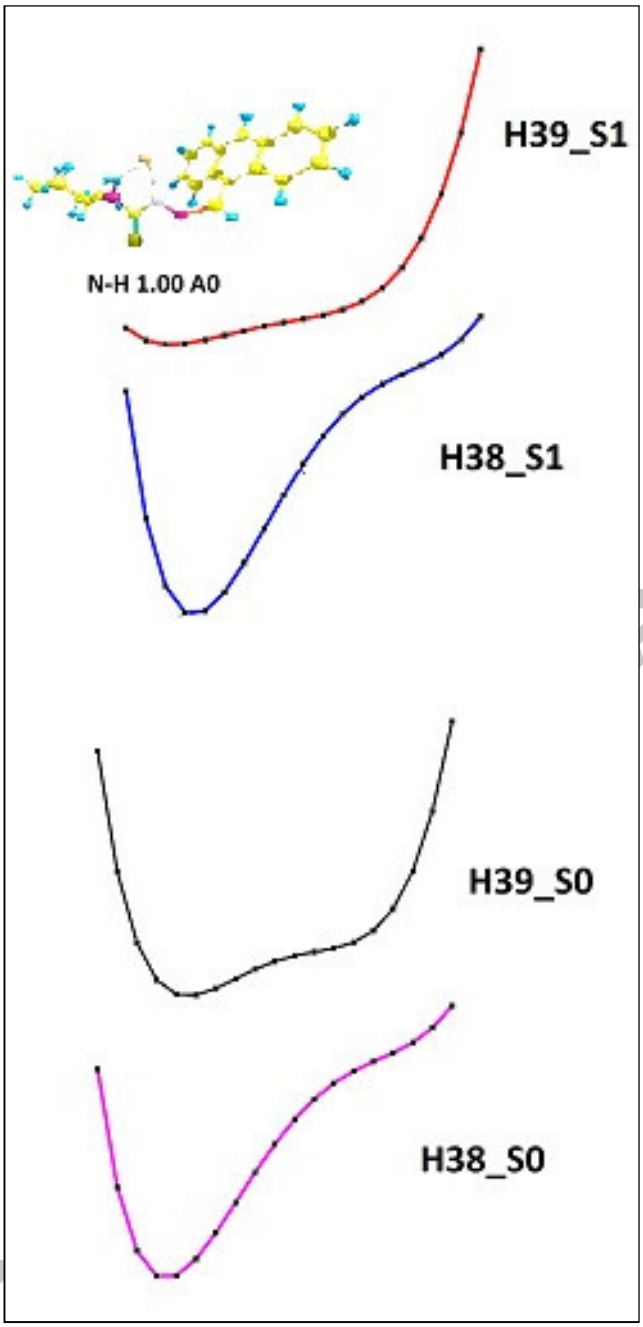

Fig 14: The sensing binding mode and mechanism of receptor towards fluoride and copper ions

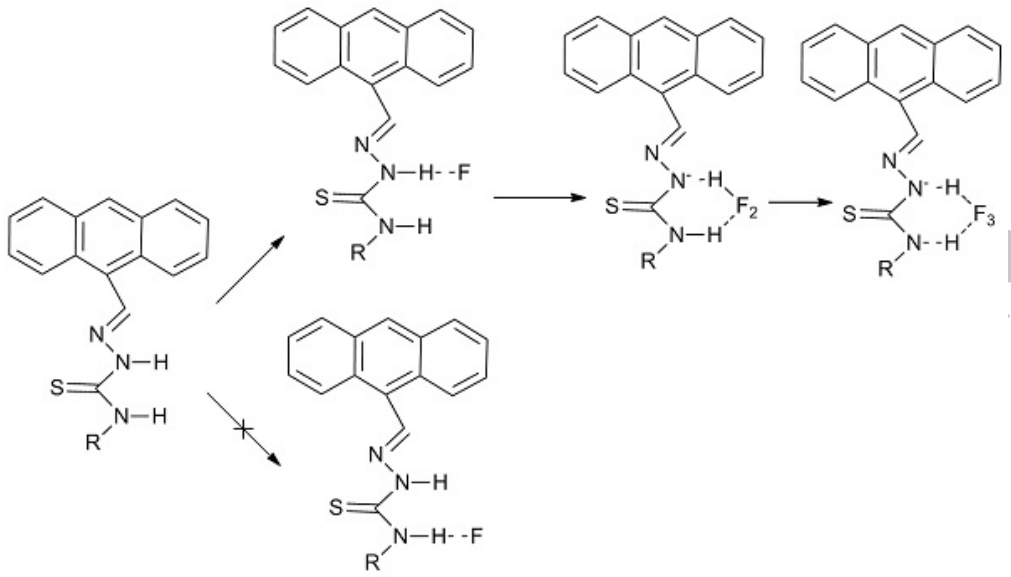

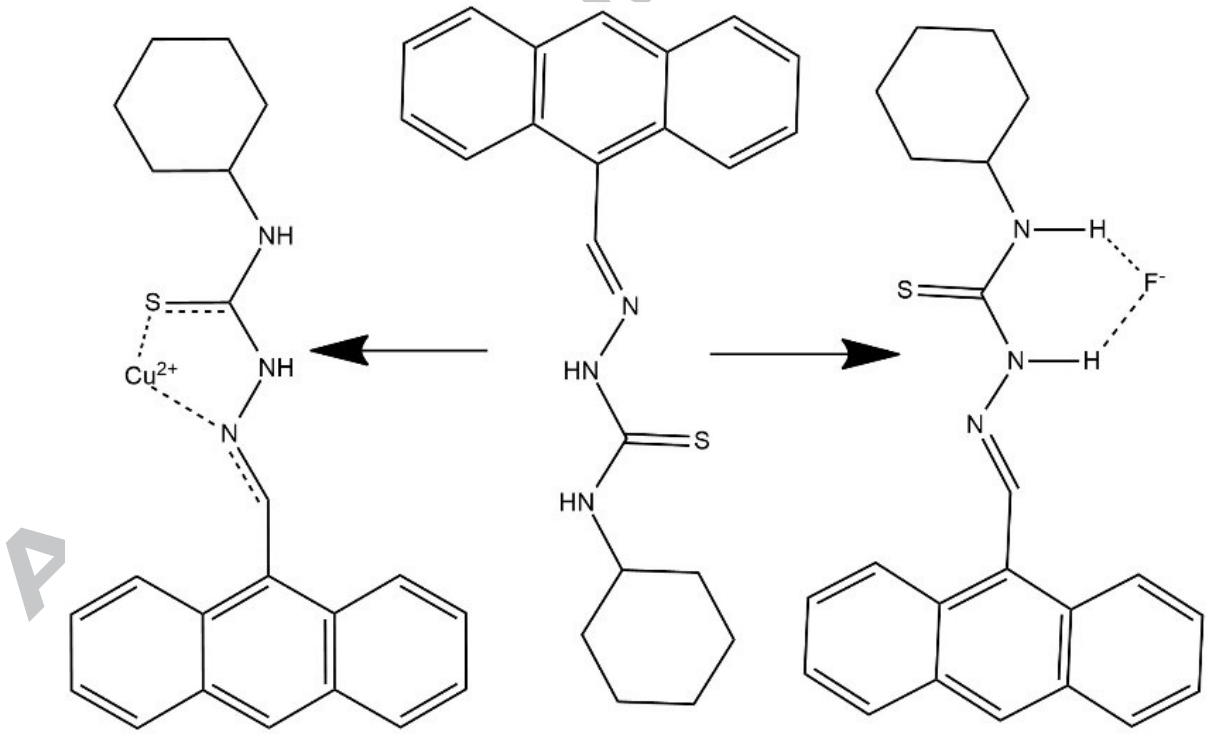

Table 1. Crystal data and structure refinement parameters

Empirical formula	$C_{22}H_{23}N_3S$
Formula weight (M)	361.51
Temperature (T), K	150 K
Wave length (Mo Kα), A^0	λ=0.71073 Å
Crystal system/Space group	Monoclinic $P2_{1/n}$
Hall symbol	-P2yn
Unit cell dimensions	a=19.8559, b=8.4480, c=22.7155, α=90 β=90.1792, γ=90
Volume (V), $^0A^3$	3810.34(15)
Z, Calculated density (ρ), mg m^{-3}	8, 1.260
Absorption coefficient (m), mm^{-1}	0.180 mm^{-1}
F000 , F000'	1536.00, 1537.44
Crystal size	0.40x0.28x0.18 mm
θ Range for data collection (^{0})	$3\text{-}28^0$
Limiting indices	h=-26 →27, k=-11→11, l=-31→29
Completeness to 2θ	$2\theta_{max}$ = 58.8°, 94%
Max. and min. transmission	T_{min}= 0.890, T_{max}= 0.969
Goodness-of-fit on F^2	1.02
R indices (all data)	R_{int}=0.055, wR(F^2)=0.1080, R[F^2>2σ(F^2)]=0.050
Largest diff. peak and hole (e $Å^{-3}$)	$\Delta\rho_{max}$=0.42, $\Delta\rho_{min}$= -0.40

Table 2. (a) Selected bond length, bond angle and dihedral angles of AntCy

S(1)-C(8)	1.6981(15)	C(8)-N(9)-N(10)	119.45(13)
N(7)-C(8)	1.333(2)	N(7)-C(8)-N(9)	115.87(13)
C(8)-N(9)	1.3495(19)	N(7)-C(8)-S(1)	124.79(12)
N(9)-N(10)	1.3827(18)	N(9)-C(8)-S(1)	119.33(12)
N(10)-C(11)	1.2854(19)	C(1)-C(6)-N(7)-C(8)	-79.01(19)
C(11)-C(12)	1.466(2)	C(6)-N(7)-C(8)-S(1)	-8.7(2)
C(6)-N(7)	1.4633(19)	N(9)-N(10)- C(11)-C(12)	-176.40(14)
C(1)-C(6)-N(7)	111.02(12)	N(10)- C(11)-C(12)-C(13)	25.8(2)
C(11)-N(10)-N(9)	114.48(13)	N(10)-N(9)-C(8)-S(1)	-177.71(11)
C(6)-N(7)-C(8)	125.46(13)		

(b) Hydrogen bond geometry

D-H···A	D-H (Å)	H···A (Å)	D···A (Å)	D···H-A (^{0})
N7-H71···N10	0.829(18)	2.201(19)	2.6112(19)	110.6(14)
N9-H91···S2	0.860(17)	2.512(18)	3.3218(14)	157.2(15)
N32-H321···N35	0.846(18)	2.2226(18)	2.6375(19)	110.0(14)
N34-H341···S1	0.86(2)	2.61(2)	3.4377(14)	160.7(15)

Table 3: Bond Characters (at ground and excited state) of AntCy and its complex of fluoride and copper

	N_1-H_1	H_1-N_1-C	N_2-H_2	H_2-N_2-C	C=S	N-N-C-S	N-N-C-N	H2-N-C-N	F-H_1	F-H_2	F-H_2-N_2	Cu-S	Cu-N	S-Cu-N
A	1.02	35.65	1.01	35.79	1.68	3.30	0.01	0.01	--	--	--	--	--	--
A*	1.02	118.3	1.01	118.14	1.67	7.26	3.55	3.59	--	--	--	--	--	--
AF	1.09	112.9	1.05	38.02	1.70	0.38	179.7	0.59	1.44	1.57	153.2	--	--	--
AF*	1.52	164.1	1.02	37.30	1.68	2.36	177.2	2.82	0.99	1.98	23.82	--	--	--
ACu	1.02	35.66	1.01	35.78	1.77	1.05	179.4	2.11	--	--	--	2.41	2.06	83.55
ACu*	1.02	35.66	1.01	35.78	1.76	0.07	179.7	2.09	--	--	--	2.37	2.06	83.75

Table 4. Absorption details of AntCy and its complex with fluoride ion and copper ion

E eV	**λ nm**	**Transition**	**%**	**E eV**	**λ nm**	**Transition**	**%**	**E eV**	**λ nm**	**Transition**	**%**
A : -1413.11583147 A.U					AF: -1513.00338034 A.U			ACu: -1251.86778511 A.U			
3.38	366.55	H→L	100	3.32	373.17	H → L	100	1.42	571.0	H → L	22.82
3.99	310.37	H-3→L	32.46	3.95	313.60	H-3 → L	24.18			H-1 → L	22.77
4.04	306.58	H-1→L+2	33.97	3.99	310.51	H-4 –→L	27.78	1.50	523.8	H-3 → L	22.01
4.48	276.48	H-2→L	35.00			H → L+1	24.85				
4.67	265.00	H-1→L	50.62	4.09	302.42	H-1 → L	25.88	1.60	408.1	H-3 → L	11.11
4.86	254.95	H→L+1	32.23			H-1→L+2	25.22				
		H→L+2	46.78	4.54	273.02	H-2 → L	25.08				

Table 5: The fluorescence emissions for the AntCy and F-complexes

E eV	**λ nm**	**f**	**Transition**	**%**	**E eV**	**λ nm**	**f**	**Transition**	**%**
A= -1413.13021575 A.U					AF= -1513.03124466 A.U				
2.646	468.53	0.3660	L→H	100	1.775	698.23	0.255	L→H	85.02
3.671	337.71	0.0266	L→H-1	35.93	2.884	429.90	0.168	L→H-1	37.47
3.810	325.40	0.0339	L→H-4	57.56	3.315	374.00	0.000	L→H-2	35.90
			L+2→H	42.43				L →H-1	32.09
3.904	317.54	0.0857	L→H-2	25.03	3.617	342.69	0.043	L+1→H	31.37
4.411	281.07	0.1187	L+1→H	59.30	3.697	335.34	0.077	L→H-4	23.87
4.433	279.69	0.0203	L→H-3	22.38	3.862	321.01	0.072	L→H-2	47.79
			L→H-2	24.58					

Table 6: Second perturbation energy of donor- acceptor interaction at ground and excited states of AntCy-F and ground state of AntCy-Cu complex

Donor (i)	Acceptor (j)	Interaction	E2 kcal/ mol	ε(j)- ε (i) a.u.	F(i,j) a.u.	Donor (i)	Acceptor (j)	Interaction	E2 kcal/ mol	ε(j)-ε (i) a.u.	F(i,j) a.u.
AF_S0: Ground State						**AF_S1: Excited state**					
CR (1) F 50	BD*(1) N 25 -H 32	σ -σ*	2.85	24.74	0.245	CR (1) F 50	LP*(1) H 32	σ -σ*	11.80	24.62	0.547
CR (1) F 50	BD*(1) N 27-H 31	σ -σ*	1.43	24.77	0.172	LP (1) F 50	LP*(1) H 32	n-σ*	14.15	0.86	0.112
LP (1) F 50	BD*(1) N 25 -H 32	n-σ*	6.65	1.19	0.082	LP (2) F 50	LP*(1) H 32	n-n*	14.61	0.84	0.112
LP (1) F 50	BD*(1) N 27 -H 31	n-σ*	3.77	1.23	0.062	LP (3) F 50	LP*(1) H 32	n-n*	3.41	0.63	0.046
LP (3) F 50	BD*(1) N 27 -H 31	n-σ*	29.4	0.72	0.130	LP (4) F 50	LP*(1) H 32	n-n*	356.30	0.86	0.513
LP (4) F 50	BD*(1) N 25 -H 32	n-σ*	59.2	0.92	0.208	CR (1) N 25	LP*(1) H 32	σ -n*	1.56	14.40	0.152
LP (4) F 50	BD*(1) N 27 -H 31	n-σ*	12.2	0.95	0.097	LP*(1) H 32	RY*(1) F 50	n-n*	1.91	1.59	0.103
A-Cu_Ground state											
LP (2) S 29	LP*(7)Cu 50	n-n*	14.6	0.61	0.120	LP (1) N 24	LP*(8)Cu 50	n-n*	18.67	0.62	0.136
LP (1) N 24	LP*(7)Cu 50	n-n*	24.3	0.75	0.173	LP (2) S 29	BD*(1) S 29 -Cu 50	n- σ*	20.78	0.61	0.144

Graphical abstract:

A schematic representation of sensing mode of AntCy towards copper and fluoride ions. The fluoride ion forms a hydrogen bond with NH proton near to the anthracene moiety. The optimised N-H bond length in excited state proton transfer is at 1.00 Å, which is confirmed by PES and NBO studies.